Structure of Raw Starch-Digesting *Bacillus cereus* β-Amylase Complexed with Maltose[†,‡]

Bunzo Mikami,*[,§] Motoyasu Adachi,[§] Takihiro Kage,[§] Elif Sarikaya,[§,||] Takashi Nanmori,[⊥] Ryu Shinke,[⊥] and Shigeru Utsumi[§]

Research Institute for Food Science, Kyoto University, Uji, Kyoto 611-0011, Japan, and Department of Agricultural Chemistry, Faculty of Agriculture, Kobe University, Rokkodaicho, Nada-ku, Kobe 657-8501, Japan

Received December 15, 1998; Revised Manuscript Received March 29, 1999

ABSTRACT: The crystals of β-amylase from *Bacillus cereus* belong to space group $P2_1$ with the following cell dimensions: $a = 57.70$ Å, $b = 92.87$ Å, $c = 65.93$ Å, and $\beta = 101.95°$. The structures of free and maltose-bound β-amylases were determined by X-ray crystallography at 2.1 and 2.5 Å with *R*-factors of 0.170 and 0.164, respectively. The final model of the maltose-bound form comprises 516 amino acid residues, four maltose molecules, 275 water molecules, one Ca^{2+}, one acetate, and one sulfate ion. The enzyme consists of a core $(\beta/\alpha)_8$-barrel domain (residues 5−434) and a C-terminal starch-binding domain (residues 435−613). Besides the active site in the core where two maltose molecules are bound in tandem, two novel maltose-binding sites were found in the core L4 region and in the C-terminal domain. The structure of the core domain is similar to that of soybean β-amylase except for the L4 maltose-binding site, whereas the C-terminal domain has the same secondary structure as domain E of cyclodextrin glucosyltransferase. These two maltose-binding sites are 32−36 Å apart from the active site. These results indicate that the ability of *B. cereus* β-amylase to digest raw starch can be attributed to the additional two maltose-binding sites.

β-Amylase catalyzes the liberation of β-anomeric maltose from the nonreducing ends of starch and is distributed in plants and microorganisms (*1*). β-Amylases from *Bacillus polymyxa* (*2*), *Bacillus circulans* (*3*), *Clostridium thermosulfurogenes* (*4*), and *Bacillus cereus* (*5*, *6*) have been cloned and sequenced. These bacterial β-amylases have properties different from those of the plant enzymes in terms of optimum pH, specific activity, isoelectric points, the number of sulfhydryl/disulfide groups, and the ability to digest raw starch, though they exhibit similar molecular weights (*7*). The ability to bind and digest raw starch granules that is found in bacterial β-amylases can be attributed to their C-terminal region, which does not show any similarity to the C-terminal region of plant amylases but has homology with the C-terminal raw starch-binding domain reported in glucoamylase, cyclodextrin glucosyltransferase (CGTase[1]), and maltotetraose producing α-amylase (*5*, *8*). The X-ray crystallographic and NMR analyses revealed two sugar-binding sites in CGTase domain E (*9*, *10*) and in the separated starch-binding domain of glucoamylase (*11*). It was pointed out, however, that the raw starch-digesting ability of some α-amylases without the C-terminal starch-binding domain may be attributed to their extra sugar-binding sites in the catalytic domain. In pancreatic α-amylase, carbohydrate recognition sites (*12*, *13*) or an accessory site (*14*) has been characterized by X-ray crystallography. A recent study about barley α-amylase complexed with acarbose also demonstrated a surface-located starch granule-binding site characteristic of cereal α-amylase (*15*). Irrespective of the starch-binding sites in the core or independent domain, they seem to be inevitable for digestion of raw starch granule.

The three-dimensional structure of soybean β-amylase (SBA) shows that the enzyme comprises the $(\beta/\alpha)_8$ core domain and a C-terminal loop region (*16*). Two maltose molecules have been found to bind in tandem in the active site pocket of SBA occupying subsites 1−2 and 3−4, where two catalytic residues, Glu 186 and Glu 380, are situated between subsites 2 and 3 (*17*). The open−close movement of the flexible loop (residues 96−103 in SBA) was found to play an important role in the catalytic step. These amino acid residues that are important for catalysis and the binding of the substrate are well-conserved between plant and bacterial enzymes (*17*), though only 29% identical residues are found between *B. cereus* β-amylase (BCB) and SBA even in the core domain (*5*).

Chemical analysis showed that one disulfide bridge and one sulfhydryl group exist in BCB (*18*) and *B. polymyxa*

[†] This work was supported in part by a Grant-in-Aid for Scientific Research from the Ministry of Education, Science, and Culture of Japan.

[‡] Atomic coordinates of the protein structures reported in this paper have been deposited with the Protein Data Bank at Brookhaeven National Laboratories under file names 1B9Z and 1B90 for the maltose-bound and free β-amylases, respectively.

* Corresponding author. Telephone: 81 (774) 38-3763. Fax: 81 (774) 38-3764. E-mail: mikami@soya.food.kyoto-u.ac.jp.

[§] Kyoto University.

[||] Research associate in Research Institute for Food Science, Kyoto University, on leave from Biochemistry, Ankara University, Turkey.

[⊥] Kobe University.

[1] Abbreviations: BCB, *B. cereus* β-amylase; SBA, soybean β-amylase; Glc, glucose; CGTase, cyclodextrin glucosyltransferase.

10.1021/bi9829377 CCC: $18.00
Published on Web 05/13/1999

β-amylase (*19*), in contrast to the plant enzymes which contain several free sulfhydryl groups (*1*). One free sufhydryl group of Cys 331 in BCB exhibits a common target site of SH reagents with the plant enzymes (*18*). Cys 91 in BCB forming the disulfide bridge exists near the flexible loop. This flexible loop carries asparatic acid and valine residues which interact with glucose residues at subsites 1 and 4, respectively (*17*). The disulfide bridge of BCB (Cys 90−Cys 99), however, has been thought to stabilize the flexible loop (residues 91−97) without affecting the open−close movement (*18*). A precise comparison of the structure between BCB and SBA will elucidate not only the role of the starch-binding domain but also the different catalytic properties that occur as a result of structural change in the core domain.

In this paper, we describe the structures of *B. cereus* β-amylase and its complex with maltose. We found two maltose-binding sites in addition to the active site, one in the starch-binding domain and the other in the core domain 32 Å away from the catalytic site.

MATERIALS AND METHODS

Assay Method. β-Amylase activity was measured in 0.1 M phosphate buffer (pH 7.0) using 0.5% potato amylopectin as a substrate, according to the modified Bernfeld method (*20*), as described previously (*18*). One unit of activity is defined as the amount of the enzyme needed to produce 1 μmol of maltose per minute. The amount of protein of the purified enzyme was determined by use of an absorption coefficient $E_{1\%,280nm}$ of 19.7 for BCB (*18*). SBA (isozyme 2) was prepared as described previously (*21*).

Expression of the BCB Gene in Escherichia coli. Construction of an expression plasmid for the *B. cereus* β-amylase DNA sequence encoding a mature β-amylase (*7*) was amplified by PCR using primers N (5′-ACCATGGCTGTAAATGGAAAAGGAATG-3′) containing an *Nco*I site and C (5′-TTAAGCTTTTACCAACTACTTGTATGAGA-3′) containing a *Hin*dIII site. PCR was conducted on the plasmid containing the gene (*5*) with reagents supplied in a kit form (Takara) with a DNA thermal cycler (Perkin-Elmer). A PCR cycle consisted of denaturation at 95 °C for 30 s, annealing at 50 °C for 1 min, and extension at 72 °C for 3 min. After 25 cycles, the products were separated by electrophoresis on a 1.2% (w/v) agarose gel and purified by using glass powder (Takara). The resultant 1.5 kb fragment was cut with *Nco*I and *Hin*dIII and inserted between the *Nco*I and *Hin*dIII sites of expression vector pET21d (Novagen) to generate plasmid pEBBA. After the cDNA sequence in the pEBBA was sequenced, the expression plasmid pEBBA was transformed into *E. coli* strain HMS174 (DE3). Four hundred milliliters of LB medium containing 20 mM $CaCl_2$ was inoculated with 4 mL of overnight-grown cultures of HMS174 (DE3) harboring pEBBA and cultured at 37 °C. At an A_{600} of 0.8, the medium was cooled to 18 °C, and IPTG was added to a final concentration of 1 mM. After cultivation for 48 h at 18 °C, the induced cells were harvested by centrifugation. The cells were suspended in the extraction buffer [50 mM sodium phosphate buffer (pH 7.0) containing 1 mM EDTA and 100 mM NaCl] and disrupted by sonication at 4 °C. After sonication, β-mercaptoethanol was added to a final concentration of 50 mM and then the mixture centrifuged at 10000*g* for 20 min.

Purification and Enzyme Properties. β-Amylase was purified from the supernatant of the cell extract by hydrophobic chromatography with Toyoperl and by CM-Sephadex ion-exchange chromatography as described previously for the purification of the enzyme from *B. cereus* BQ 10-S1 Spo III (*18*). Approximately 200 mg of purified enzyme was obtained from 4 L of cell broth. The purified enzyme exhibited a specific activity 1.5-fold higher than the specific activity of that purified from *B. cereus* BQ 10-S1 Spo III (*18*). The molecular weight was determined to be 58 300 by MALDI-TOF mass spectrometry using sinapinic acid as a matrix with a Voyager RP mass spectrometer (PerSeptive Biosystems). The N- and C-terminal amino acid sequences analyzed by Procise 492 and Procise C 494 sequencers (Applied Biosystem) were found to be AVNGK and XXW, respectively, which were consistent with the reported cDNA sequence of BCB (*5*). The calcium content was determined by atomic absorption spectrometry with a Hitachi Z-8270 atomic absorption spectrometer.

Crystallization. β-Amylase crystals were grown at 18 °C by the hanging-drop vapor-diffusion method employing 5 μL of a 10 mg/mL protein solution [0.1 M acetate buffer (pH 4.6)] mixed with 5 μL of precipitant solution [18% PEG6000, 5% saturated $(NH_4)_2SO_4$, and 0.1 M acetate buffer (pH 4.6)]. Hexagonal or quadrilateral plate crystals appeared in a few days and grew up to 1 mm × 0.5 mm × 0.3 mm. These crystals are monoclinic, belonging to space group $P2_1$ with the following cell dimensions: $a = 57.70$ Å, $b = 92.87$ Å, $c = 65.93$ Å, $\beta = 101.95°$, and $Z = 2$.

Data Collection. The crystal used for data collection was the largest available and had approximate dimensions of 0.5 mm × 0.5 mm × 0.3 mm. The crystal data in the presence or absence of 200 mM maltose were collected up to 2.0 and 2.4 Å resolution, respectively. For heavy atom derivatives, the crystal data were collected around 3−2.9 Å resolution immediately after soaking in a heavy atom solution [2 mM K_2PtCl_4, 1 mM CH_3HgOH, and 5 mM $Ac_2(UO)_2$, containing 200 mM maltose in the bottom solution] for 1 h at 18 °C. X-ray data were collected at room temperature using CuKα radiation ($\lambda = 1.5418$ Å) with a Siemens Hi-Star area detector coupled to MAC Science M18XHF rotating anode generator.

Structure Determination. The structure was determined by the multiple isomorphous replacement method using the Phase 97 program package (*22*). The derivative data sets were scaled by CMBISO. Heavy atom positions were determined at 2.9 Å resolution by difference Patterson and by difference Fourier maps. The heavy atom parameters were refined at 2.9 Å by PHASIT (Table 1). The mean figure of merit was 0.57 for 11 957 reflections. Solvent flattening (*23*) implemented in Phase 97 was applied to the isomorphous replacement phase with an assumed solvent volume fraction of 55%. The final *R*-factor and the figure of merit were 0.27 and 0.82 for 11 951 reflections, respectively. The resultant map was of a high enough quality to locate each amino acid residue by a graphic program of Turbo-Frodo (Biograph). The flexible loop and three maltose molecules, except for that in the starch-binding domain, were clearly visible in this map. Refinement of the protein model by simulated annealing and then positional and *B*-factor refinement, using X-PLOR

Table 1: Summary of Statistics for Heavy Atom Derivatives

derivative	resolution (Å)	*R*-Cullis	*R*- Kraut	phasing power	heavy atom	site *x*	site *y*	site *z*	occupancy	*B* (Å^2)	binding site
$Ac_2(UO_2)$	3.1	0.593	0.106	1.60	U-1	0.129	0.000	0.197	0.612	73.30	D60, K140, E144
					U-2	0.967	0.063	0.804	0.216	50.00	E32
					U-3	0.311	0.402	0.256	0.202	50.00	E24
K_2PtCl_4	2.9	0.700	0.131	1.11	Pt-1	0.723	0.045	0.825	0.887	80.00	M242, E238
					Pt-2	0.200	0.376	0.922	0.423	80.00	M248
CH_3HgOH	2.9	0.685	0.105	1.34	Hg-1	0.969	0.056	0.518	0.552	48.16	H512
					Hg-2	0.675	0.383	0.294	0.791	80.00	C339
					Hg-3	0.069	0.038	0.807	0.638	80.00	C99
					Hg-4	0.244	0.380	0.728	0.625	80.00	H463

Table 2: Statistics of Data Collection and Refinement of BCB−Maltose and BCB

space group	$P2_1$	$P2_1$
inhibitor	maltose (200 mM)	−
cell dimensions		
a, *b*, *c* (Å)	58.16, 93.74, 66.66	57.70, 92.87, 65.93
β (deg)	102.44	101.95
data collection		
no. of measured reflections	92118	59931
no. of unique reflections ($\|I\| > 1\sigma I$)	39463	24292
R_{sym} (%)	4.6	7.3
completeness (%)		
data to 2.5 Å resolution	95.2	98.8
data to 2.0 Å resolution	83.4	−
refinement		
resolution range (Å)	11.0−2.1	15.0−2.5
no. of reflections used ($\|F\| > 2\sigma F$)	33365 (82.3%)	19491 (84.7%)
no. of residues/no. of waters	516/275	516/120
no. of maltoses	4	−
no. of calciums	1	1
no. of acetates	1	1
no. of sulfates	1	1
L3 loop 1 conformation	closed	open
average *B*-factor (Å^2)	23.0	19.1
rms deviation		
bond lengths (Å)	0.015	0.013
bond angles (deg)	3.08	3.12
R-factor (%)	17.0	16.4
free *R* (%)	22.1	24.7

version 3.1 (*24*), has resulted in a final *R* of 0.215 for the data between 10.0 and 2.3 Å resolution. Four maltose molecules and visible water molecules having more than 4σ on the $|F_o| - |F_c|$ map were then added to the model. Several cycles of positional and *B*-factor refinements followed by the model rebuilding were carried out at 2.1 Å until no further improvements were made to the model. The final model consisted of 516 amino acid residues, four maltose molecules, one calcium ion, one sulfate ion, one acetate ion, and 275 water molecules with an *R* of 0.170 ($R_{free} = 0.221$) for 33 365 reflections when $F > 2\sigma(F)$ between 11.0 and 2.1 Å resolution. For the refinement of the crystal without maltose, the protein model of the BCB−maltose complex was used for the initial model. After rigid-body refinement, the open flexible loop could be fitted into its $|F_o| - |F_c|$ electron density map. Rigid-body refinement, refinement by simulated annealing and then positional and *B*-factor refinement, has resulted in a final *R* of 0.186 for the data between 15.0 and 2.5 Å resolution. The final model consists of 516 amino acid residues, one calcium ion, one sulfate ion, one acetate ion, and 120 water molecules with an *R* of 0.164 ($R_{free} = 0.247$) for 19 491 reflections when $F > 2\sigma(F)$ between 15.0 and 2.5 Å resolution. For the identification of the calcium site, an anomalous difference Fourier map was calculated by Phases 97 with 15−2.8 Å resolution data (86% complete pairs).

RESULTS

Quality of the Final Models. The final statistics for the refinements of BCB−maltose and BCB together with statistics for data collection are shown in Table 2. The BCB−maltose model was built from the solvent-flattened MIR map and refined at 2.1 Å resolution with an *R*-factor of 17.0%. The BCB model was also refined at 2.5 Å resolution with an *R*-factor of 16.4%. The final model of BCB−maltose contains 516 amino acid residues, 275 water molecules, four maltose molecules at three different binding sites, one sulfate ion, one acetate ion, and one calcium ion. The final model of BCB is the same, except for there being 120 water molecules and no maltose. These models have good geometries and absolute positional errors of 0.22 and 0.25 Å, respectively, as estimated from Luzatti plots (*25*). Ramachandran plots of the main chain conformation angles show that about 88% lie within the core region, with 100% lying within the allowed region for both models (*26*, *27)*. The average *B*-factors for the protein and water atoms are 21.7 and 36.8 Å^2 and 18.7 and 29.7 Å^2 for BCB−maltose and BCB, respectively. The average *B*-factor for the bound

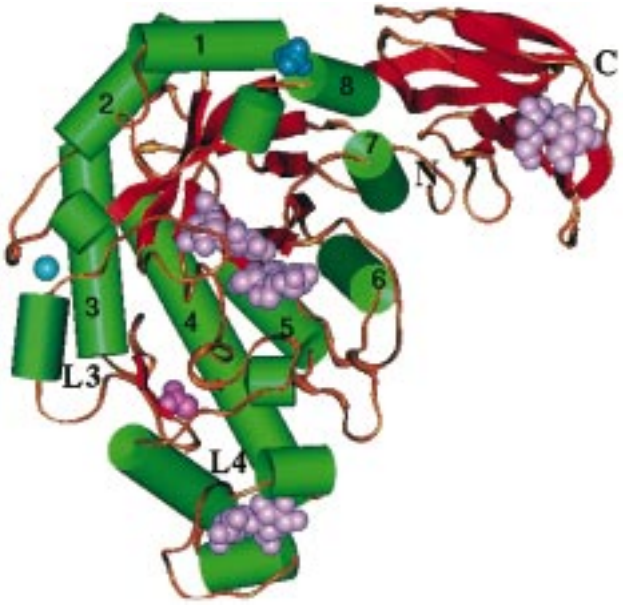

FIGURE 1: Schematic representation of *B. cereus* β-amylase using the program InsightII. The helices and strands are shown in green and red, respectively. The bound maltose (pink), calcium (cyan), acetate (purple), and sulfate (blue) are shown as sphere models. The helices in the $(\beta/\alpha)_8$-barrel are numbered.

maltose molecules of BCB−maltose is 34.5 Å^2. There are four cis peptide bonds in the structures. These are between Pro 187 and Ser 188, between Pro 341 and Glu 342, between Arg 397 and Tyr 398, and between Pro 504 and Val 505. The first and third cis peptide positions are also conserved in the structure of SBA (*16*).

Overall Structure of BCB. BCB consists of two domains, an N-terminal core, and a C-terminal starch-binding domain. Figure 1 shows the ribbon diagram of the overall structure of the BCB−maltose complex with calcium, acetate, and sulfate ions. The core domain has a $(\beta/\alpha)_8$ supersecondary structure similar to that of SBA (*16*). However, BCB possesses a starch-binding domain immediately following helix 8 (α8), whereas SBA has a long C-terminal loop. The C-α rms distance between BCB and BCB−maltose was 0.44 Å for the 511 common C-α atoms except for the flexible loop region. In the flexible loop (residues 91−97), BCB has an open loop conformation, whereas BCB−maltose has a closed loop conformation as reported for SBA and SBA−maltose structures (*17*).

Figure 2 shows the sequence alignment between BCB and SBA in the core region and that between the BCB C-terminal domain and the starch-binding domains of CGTase (domain E) and glucoamylase. In the core region, BCB has an amino acid identity of 29% with respect to SBA (*16*), but the residues involved in catalysis and binding of the substrate are highly conserved, as shown in the four boxes of Figure 2. There are four deletion regions of more than five residues and one insertion of 16 residues in the BCB sequence. In the C-terminal starch-binding domain, BCB exhibits 31 and 22% amino acid residue identity with respect to CGTase (*9*) and glucoamylase (*11*, *28*), respectively.

Core Domain. A comparison of the core domain between BCB and SBA shows a C-α rms distance of 1.21 Å with 352 common residues within a distance of 2.4 Å as shown in Figure 3A. Though the main secondary structure elements are common in both enzymes, there are several insertions and deletions as shown in Figures 2 and 3A. BCB has L1 (the loop connecting β1 and α1) which is three residues shorter than SBA at residues 20−26. In the loop−helix−loop motif of L3, this extra helix (L3α) is shorter and changed to a loop of residues 109−112. One loop of seven residues at the beginning of α3 in SBA is omitted in BCB at residue 133. Just after L4α, one more helix of eight residues and a successive loop of nine residues are inserted in BCB at residue 213, and one loop of 10 residues found in SBA is deleted in BCB at residue 237. These successive insertion and deletion regions from residue 212 to 243 make a hook-like structure which forms a novel maltose-binding site (dotted box in Figure 2). Two residues are inserted in L5 at residue 297, and two loops of five residues and one loop of 11 residues in SBA are deleted at residue 311, just before α5, and residue 387 at the end of α7, respectively. In contrast to SBA, one calcium-binding site was found in the region surrounded by L2 and α3 (Figures 1 and 3A). The presumed acetate-binding site was found in a small cleft surrounded by L3 loop 2, L4 loop 1, L4 helix, and α4 (Figures 1 and 3A). One sulfate-binding site was also found at the beginning of α8 in the interface of a symmetry molecule (Figures 1 and 3A).

Starch-Binding Domain. The C-terminal starch-binding domain comprises 99 residues from residue 418 to 516, and is folded into two four-stranded antiparallel β-sheets (βa and βb in Figure 2) which forms an eight-stranded antiparallel β-barrel (Figures 2 and 3B) as has been reported for CGTase (*29*) and a separated starch-binding domain from glucoamylase (*30*). Figure 3B represents the C-α positions of the starch-binding domain superimposed onto that from CGTase (domain E) (*9*). The secondary structure of the starch-binding domain in BCB is essentially the same as that of domain E in CGTase. The C-α rms distance was 0.53 Å for 80 common C-α atoms within 2.4 Å. Their structures were slightly different at residues 461−466 near maltose-binding site 1, and also at residues 453, 488, 493, 498, and 503 by one residue insertion, and at 458 and 507 by one residue deletion in the BCB sequence (Figure 2). When the structure is compared with the starch-binding domain from glucoamylase (*30*), the C-α rms distance increases to 1.40 Å for 65 common C-α atoms within 2.5 Å, suggesting that the domain of BCB closely resembles domain E of CGTase.

The core domain interacts with the C-terminal domain at the N-terminus, α7 and α8. There are seven interdomain hydrogen bonds: two with the N-terminus [Ala 1 N···Tyr 454 O (2.8 Å) and Gly 4 O···Gln 457 N (2.8 Å)], two with α7 [Glu 383 O-ϵ1···Ser 448 O-γ (3.1 Å) and Asn 387 O-δ1···Ala 444 O (2.8 Å)], and three with α8 [Lys 412 O···Arg 477 N-η2 (2.8 Å), Asp 413 O···Arg 443 N-η1 (3.0 Å), and Asp 413 O···Arg 443 N-η2 (2.9 Å)]. These interactions support and fix the relative orientation of the C-terminal domain to the core domain. In the SBA core structure, eight N-terminal residues (residues 5−12), L7 (residues 401−411), and the beginning (443−447) and ending (484−494) of the C-terminal loop occupy the position of the C-terminal domain of BCB (Figure 3A). BCB has a bent N-terminus (residues 1−11), and L7 is deleted to avoid an interdomain collision.

Active Site in the Core Domain. In the BCB−maltose complex, L3 loop 1 takes on a closed conformation and the

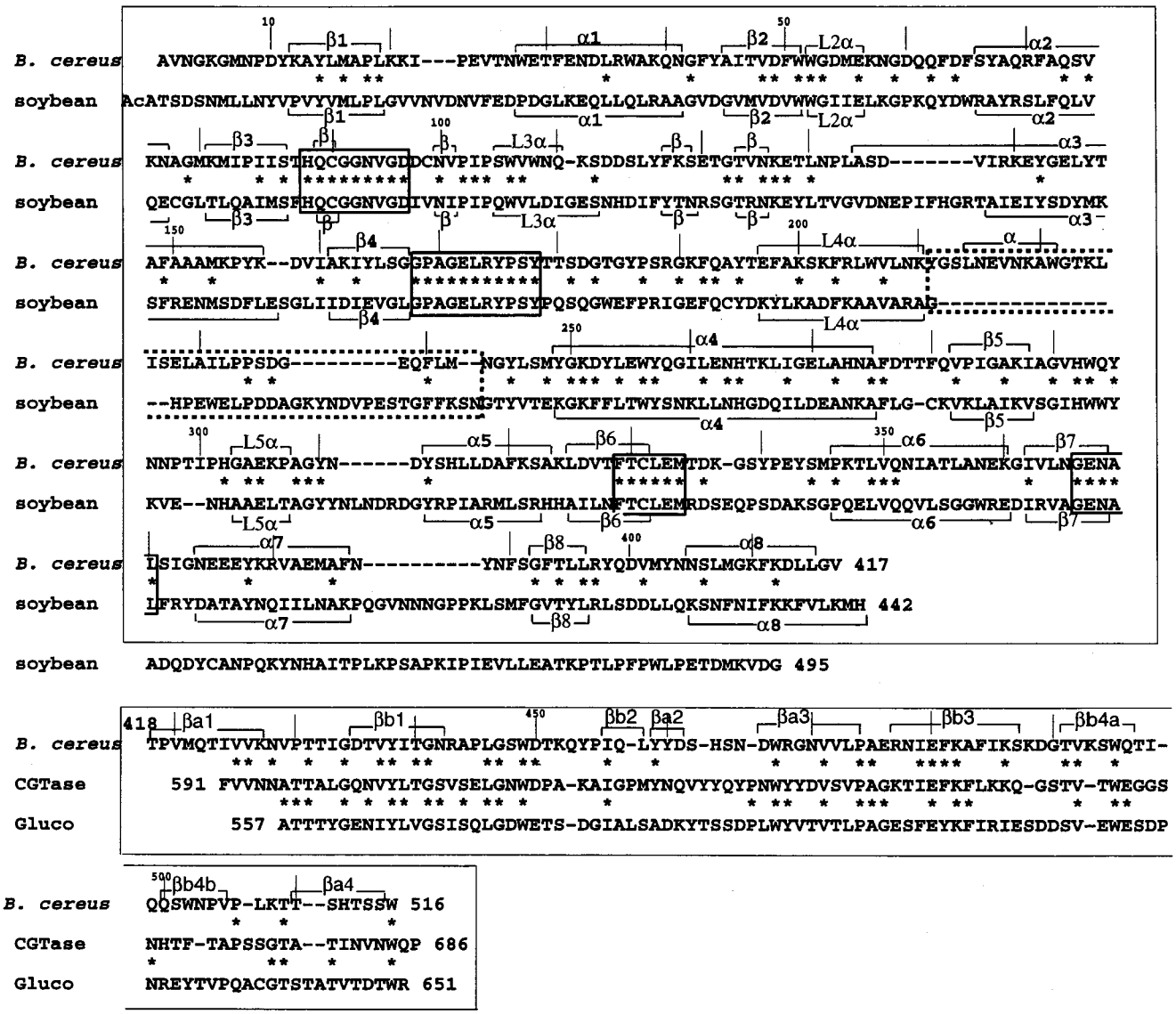

FIGURE 2: Alignment of the BCB sequence with SBA (*35*, *36*) in the core region and that with CGTase (*9*) and glucoamylase (*28*) in the C-terminal domain region. The residues of helices and strands are represented as α and *β*, respectively. The helices and strands in an $(\beta/\alpha)_8$-barrel and strands in a C-terminal domain are numbered. Four highly conserved regions in the core are boxed with a thick line, and residues 211−242 in BCB which form the second maltose-binding site are boxed with a dotted line.

two maltose molecules bind in tandem as has been reported for the structure of the SBA−maltose complex (*17*), whereas that of free BCB takes on an open conformation. Figure 4A shows the bound maltose molecules and the surrounding amino acid residues interacting with the maltose, together with those of SBA. The bound maltose position is almost the same as that of the SBA−maltose complex at subsite 1 (Glc 1), but is slightly different at subsites 2−4 (Glc 2, Glc 3, and Glc 4). The data listed in Table 3 represent the interactions of protein atoms with the bound maltose molecules in the BCB−maltose complex. There are seven, six, and six direct hydrogen bonds between protein atoms and OH groups of Glc 1, Glc 2, and Glc 3, respectively, but only one hydrogen bond between OH-3 of Glc 4 and N-ϵ2 of His 292 was found at subsite 4. Besides the direct hydrogen bonds with protein atoms, six water-mediated hydrogen bonds were found at Glc 1 [O-2···Wat 620···Val 95 O (2.7 and 2.9 Å), O-3···Wat 618···Gln 90 O (2.8 and 2.9 Å), and O-6···Wat 603···Thr 47 O-γ (3.1 and 3.1 Å)], Glc 2 [O-3···Wat 620···Val 95 O (3.1 and 2.9 Å) and O-3···Wat 712···Ala 369 O (3.1 and 2.9 Å)], and Glc 4 [O-6···Wat 678···Tyr 186 N (2.9 and 3.1 Å)]. Two catalytic residues, Glu 172 and Glu 367, have the same configuration as those described for Glu 186 and Glu 380 in the SBA−maltose complex (*17*). Glu 172 makes hydrogen bonds with O-5 of Glc 2, O-4 of Glc 3, and O-6 of Glc 3, whereas Glu 367 does the same with O-6 of Glc 2. In contrast to the hydrogen bonds, many van der Waals contacts of Glc 4 with Tyr 186, Leu 370, and Trp 293 were found (Table 3). One remarkable difference between BCB and SBA was found around subsite 4. BCB does not have the side chains which correspond to Gln 194 and Trp 198 in SBA. In SBA, Trp 198 makes a contact with Glc 4, and N-ϵ2 of Gln 194 makes a hydrogen bond with O of Gly 97 on the closed flexible loop. The position of the loop of residues 180−184 in BCB differs by about 3.5 Å from the corresponding loop in SBA. This is because a loop between residues 235 and 245 in SBA which interacts and supports the 194−199 loop in SBA is deleted in BCB. The lack of the Trp residue, together with the different side chain positions of Tyr 186 and Met 334,

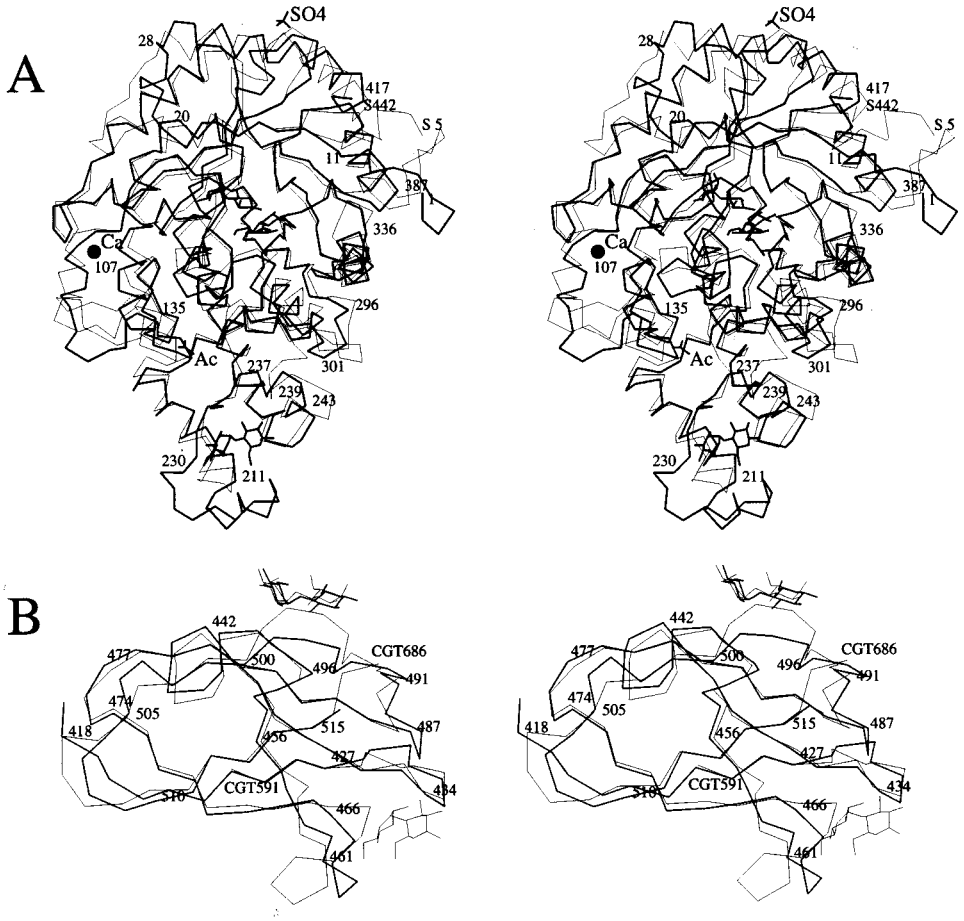

FIGURE 3: Stereodiagram of superpositions of C-α atoms of BCB with those of SBA in the core (A) and with those of CGTase domain E in the C-terminal domain (B). The superpositions were created with the RIGID program in Turbo-Frodo.

contributes to the altered positions of the bound maltose at subsites 3 and 4.

Figure 4B shows the conformational change induced by the binding of maltose. The open−close movement of the flexible loop carries Asp 97 and Val 95 by 5 and 13 Å, respectively. The right-handed disulfide bridge between Cys 91 and Cys 99 did not change conformation in each structure, as predicted from the model of SBA (*18*). In addition to movement of the flexible loop, the side chains of Tyr 164, Met 16, and Lys 287 flip by 34° (χ_2), 52° (χ_1), and 76° (χ_1), respectively. The conformational change of Lys 287 is important in accommodating the hydroxyl moiety of C-6 of the Glc 2 residue, and the movement in turn induces the side chain change of Met 16 and Tyr 164. The main chain atom positions of Thr 330 and Cys 331 are altered by 1.08 and 1.14 Å, respectively, allowing the formation of hydrogen bonds between O-γ1 of Thr 330 and O-1 of Glc 2 (2.9 Å), between O-γ1 of Thr 330 and O-3 of Glc 3 (2.7 Å), and between S-γ of Cys 331 and O-2 of Glc 3 (3.6 Å). Their side chains also flip by 65° (χ_1) and −96° (χ_1), respectively, to make these hydrogen bonds.

Maltose-Binding Sites in the Core. One maltose-binding site was found in L4 loop 2, where the sequence alignment shows an insertion of 16 residues and a deletion of 11 residues with respect to the SBA sequence (Figure 2). The inserted loop at the end of the L4 helix makes a "hook" structure which prepares a cleft surrounded by L4 loop 2 and by the beginning of α4. The reducing end of maltose (Glc 5) binds at the beginning of α4, and the nonreducing end (Glc 6) toward L4 loop 2. This maltose-binding site is about 32 Å away from the catalytic site. The main chain and side chain atoms involved in the binding of maltose are shown in Figure 5 and are listed in Table 3. O-γ of Ser 235 makes two hydrogen bonds with O-2 and O-3 of Glc 5. The main chain O of Leu 232 and Ala 230 also makes hydrogen bonds with O-4, and with both O-4 and O-6, respectively. In contrast to Glc 5, Glc 6 makes three possible hydrogen bonds only with the side chain of Gln 239. There is one water-mediated hydrogen bond with O-3···Wat 699···Gln 239 N-ϵ2 (2.6 and 2.8 Å) and Wat 699···Asp 236 O (3.0 Å). Glc 5 and Glc 6 make van der Waals contacts with Trp 221, Leu 225, and Tyr 249, and with Phe 240 and Tyr 249, respectively (Table 3). A comparison of the structures of BCB and BCB−maltose revealed that maltose induced a side chain flip on Gln 239 by 149° (χ_2) and on Ser 235 by 119° (χ_2) to form hydrogen bonds with each glucose residue.

Maltose-Binding Site in the C-Terminal Starch-Binding Domain. One maltose is found at the same maltose-binding site (site 2) of the CGTase−maltose complex (*9*), but no maltose density was observed at site 1 of the CGTase−maltose complex under the experimental conditions described here (Figure 3B). The four residues of Trp 449 and Trp 495, Gln 499, and Lys 482 interact with the maltose. Two glucose residues, Glc 7 and Glc 8, are stacked on each Trp residue and make four hydrogen bonds between Glc 7 O-2 and O-3 and O-ϵ1 of Gln 499 and between Glc 8 O-2 and O-3 and N-ζ of Lys 482, respectively (Figure 6 and Table 3). These

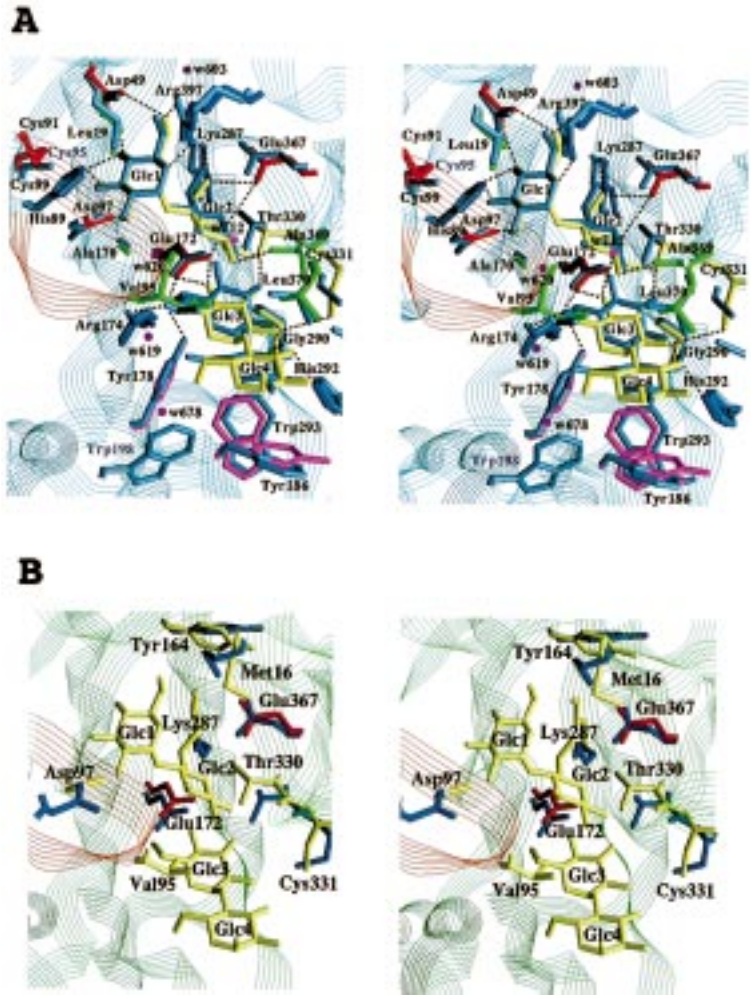

FIGURE 4: (A) Stereodiagram of the active site of BCB superimposed onto the SBA active site. The backbone structure is represented as a ribbon where the open flexible loop is red. The bound maltose is yellow. The side chains of acidic, basic, hydrophobic, and aromatic residues are red, blue, green, and purple, respectively. Corresponding residues in SBA are cyan. Water molecules related to the binding of maltose are shown as pink circles. The hydrogen bonds are shown by broken lines. (B) Stereodiagram of the conformation change induced by the binding of maltose. The backbone structure is represented as a ribbon where the open and closed flexible loops are red and blue, respectively. Maltose and the moved residues in the BCB−maltose complex are yellow. Two catalytic residues in the BCB−maltose complex are red. The corresponding residues in BCB are blue. The figure was drawn with GRASP (*37*).

features of the symmetrical binding sites for glucose are very similar to those found in CGTase domain E (*9*). Figure 6 also represents the corresponding binding site of CGTase domain E with its C-α atoms superimposed onto that of the BCB C-terminal domain. Though Gln 499 is substituted for Asn 667 in CGTase, they share a highly conserved maltose-binding site. In contrast to CGTase, we could not find any maltose density around the other maltose-binding site near Asn 627, Tyr 633, and Trp 636 in CGTase, which correspond to Tyr 460, Asn 465, and Trp 467, respectively, in BCB. The substitutions of Asn 627 and Tyr 633 in CGTase for Tyr 460 and Asn 465 in BCB may cause the reduced level of binding of maltose to BCB. A significant conformational change was also found between the loop of residues 460−465 in BCB and that of residues 627−636 in CGTase.

Conformation of the Bound Maltose Molecules. All the bound maltose molecules both in the active site and in the two starch-binding sites are in the $^4C_1$ pyranoid forms. The torsion angles defined as O5···C1−O4′−C4′ (ϕ) and C1−O4′−C4′···C5′ (ψ) between Glc 1 and Glc 2 are 62° and −145°, between Glc 3 and Glc 4 are 109° and −108°, between Glc 5 and Glc 6 are 81° and −137°, and between Glc 7 and Glc 8 are 103° and −129°, respectively. All four maltose molecules have ϕ and ψ torsion angles in the low-energy region of the isoenergy map (*31*). The torsion angles of the two maltose molecules in the active site are comparable with those reported for the SBA−maltose complex: $\phi = 67°$ and $\psi = -151°$ between Glc 1 and Glc 2 and $\phi = 112°$ and $\psi = -113°$ between Glc 3 and Glc 4 (*17*). The β-anomer configurations were assigned in Glc 2, Glc 6, and Glc 8, whereas an α-anomer configuration gave precedence over a β-anomer in Glc 4.

Calcium-, Acetate-, and Sulfate-Binding Sites. One calcium-binding site was found in a cavity facing the other side of the active site and was surrounded by L2, α3, and helix L3. Ligands are provided from L2 (O-ϵ2 of Glu 56, O-δ2 of Asp 60, and O-ϵ1 of Gln 61), from α3 (O-ϵ1 of Glu 141 and O-ϵ1 of Glu 144), and from a water (water 688) which hydrogen bonds to both O-ϵ1 of Glu 56 and O of Glu 141. Figure 7A shows the liganded side chains around the calcium ion. The six ligands are located 2.1−2.8 Å from the calcium, and make an approximate octahedron around it. This calcium has the highest density in an anomalous difference Fourier

Table 3: Interactions between Bound Sugar Atoms and Protein Atoms

hydrogen bond			contact[a]		hydrogen bond			contact[a]	
sugar atom	protein atom	distance (Å)	sugar residue	protein residue	sugar atom	protein atom	distance (Å)	sugar residue	protein residue
site 1					site 2				
Glc 1 O-2	Asp 97 O-δ1	2.6	Glc 1	His 9	Glc 5 O-2	Ser 235 O-γ	3.2	Glc 5	Trp 221
Glc 1 O-2	Wat 618 O	3.1	Glc 1	Leu 19	Glc 5 O-2	Wat 865 O	2.7	Glc 5	Leu 225
Glc 1 O-2	Wat 620 O	2.7	Glc 1	Ile 85	Glc 5 O-3	Ser 235 O-γ	3.3	Glc 5	Leu 232
Glc 1 O-3	His 89 N-ε2	2.8	Glc 1	His 89	Glc 5 O-4	Ala 230 O	2.7	Glc 5	Tyr 249
Glc 1 O-3	Wat 618 O	2.8	Glc 1	Ala 170	Glc 5 O-5	Tyr 249 O-η	3.3		
Glc 1 O-4	Asp 49 O-δ2	2.8			Glc 5 O-6	Ala 230 O	3.3		
Glc 1 O-4	His 89 N-ε2	3.1			Glc 5 O-6	Leu 232 N	3.1		
Glc 1 O-4	Wat 690 O	3.0							
Glc 1 O-6	Asp 49 O-δ1	2.9			Glc 6 O-1	Gln 239 O-ε1	3.2	Glc 6	Phe 240
Glc 1 O-6	Arg 397 N-η2	2.9			Glc 6 O-2	Gln 239 O-ε1	2.9	Glc 6	Tyr 249
Glc 1 O-6	Wat 603 O	3.1			Glc 6 O-2	Gln 239 N-ε2	3.2		
					Glc 6 O-3	Wat 699 O	2.6		
Glc 2 O-1	Thr 330 O-γ	2.9	Glc 2	Thr 330	Glc 6 O-5	Wat 770 O	2.9		
Glc 2 O-1	Wat 679 O	3.1			Glc 6 O-6	Wat 770 O	3.2		
Glc 2 O-2	Ala 369 O	2.6			site 3				
Glc 2 O-2	Wat 712 O	3.2			Glc 7 O-2	Gln 499 O-ε1	2.6	Glc 7	Trp 449
Glc 2 O-3	Val 95 O	3.2			Glc 7 O-3	Gln 499 O-ε1	3.1		
Glc 2 O-3	Wat 620 O	3.1							
Glc 2 O-3	Wat 712 O	3.1			Glc 8 O-1	Wat 827 O	2.8	Glc 8	Trp 495
Glc 2 O-3	Wat 677 O	2.8			Glc 8 O-2	Lys 482 N-ζ	3.4		
Glc 2 O-4	Wat 620 O	3.2			Glc 8 O-2	Wat 827 O	3.0		
Glc 2 O-5	Glu 172 O-ε2	3.3			Glc 8 O-3	Lys 482 N-ζ	2.8		
Glc 2 O-5	Wat 679 O	3.2							
Glc 2 O-6	Lys 287 N-ζ	3.0							
Glc 2 O-6	Glu 367 O-ε2	3.1							
Glc 3 O-2	Gly 290 O	2.9	Glc 3	Val 95					
Glc 3 O-2	Cys 331 S-γ	3.6	Glc 3	Tyr 178					
Glc 3 O-3	Thr 330 O-γ	2.7	Glc 3	Ala 289					
Glc 3 O-4	Glu 172 O-ε1	2.7	Glc 3	Trp 293					
Glc 3 O-4	Glu 172 O-ε2	2.6	Glc 3	Thr 330					
Glc 3 O-6	Glu 172 O-ε1	2.8							
Glc 3 O-6	Tyr 178 O-η	3.2							
Glc 3 O-6	Arg 174 N-η2	2.8							
Glc 4 O-3	His 292 N-ε2	2.9	Glc 4	95 Val					
Glc 4 O-6	Wat 678 O	2.9	Glc 4	Tyr 186					
			Glc 4	Trp 293					
			Glc 4	Leu 370					

[a] C−C distance of <4.5 Å.

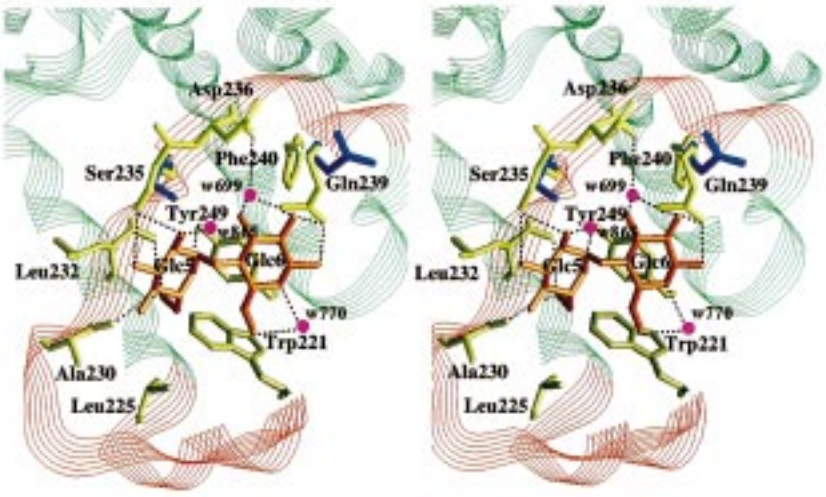

FIGURE 5: Stereodiagram of the second maltose-binding site in the core. The backbone structure is represented as a ribbon where the insertion/deletion loop (residues 211−242) is red. The bound maltose is orange. The side chains and parts of the main chain in the BCB−maltose complex are yellow. The side chain of Ser 235 and Gln 239 in BCB which change the conformations are blue. Water molecules related to the binding of maltose are shown as pink circles. The hydrogen bonds are shown as broken lines. The figure was drawn with GRASP (*37*).

map (Figure 7A). The number of bound calcium ions in BCB was also determined by atomic absorption spectrometry to be 1.2 mol/mol of enzyme, whereas that determined in SBA was <0.02 mol/mol of enzyme. This calcium-binding site seems to not be related to the calcium-binding sites found in α-amylase (*32*) and CGTase (*29*). Presumably, this

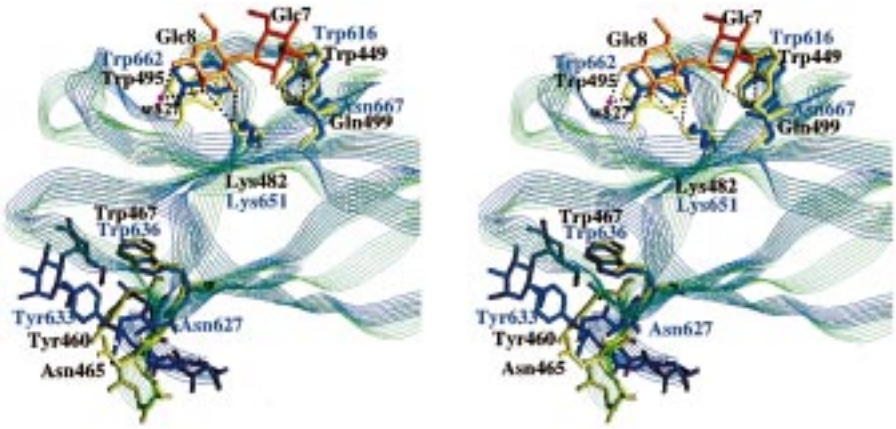

FIGURE 6: Stereodiagrams of the maltose-binding site in the C-terminal domain superimposed onto that of the CGTase E domain. The backbone structures of BCB and CGTase (*9*) are represented as green and blue ribbons, respectively. The bound maltose in the BCB−maltose complex is orange. The side chains involved in the binding of maltose in BCB and in CGTase are yellow and blue, respectively. One maltose and residues 627−636 that are blue in CGTase correspond to the vacant binding site in BCB (residues 460−467 colored yellow). The figures were drawn with GRASP (*37*).

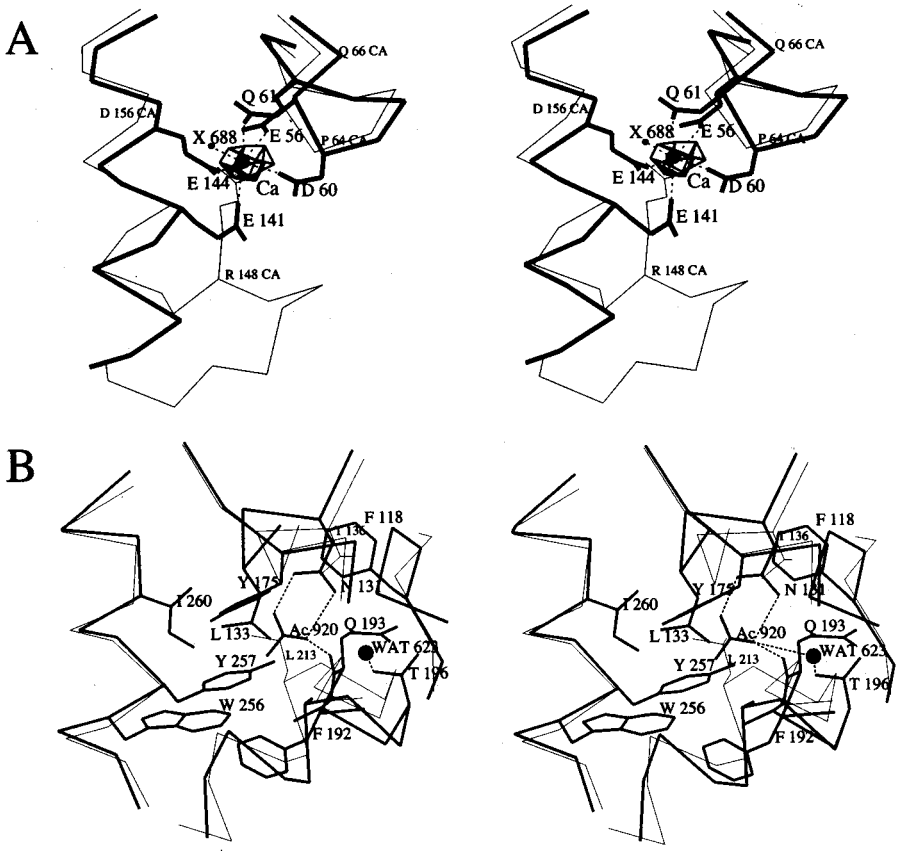

FIGURE 7: Stereodiagrams of the calcium-binding site (A) and acetate-binding site (B) which are superimposed onto the corresponding sites of SBA. The structures of BCB and SBA are represented as thick and thin lines, respectively. The small labels denote the residues of SBA. The map around the bound calcium represents the anomalous difference Fourier map contoured at 3σ calculated with 15−2.8 Å resolution data.

calcium ion is necessary for the stabilization of the conformation of L2. In SBA, the side chain of Arg 148, which is located on an inserted loop at the beginning of α3, occupies and stabilizes this negatively charged cavity instead of calcium (Figure 7A).

One acetate-binding site was found in a deep cavity surrounded by L3, L4, L4 loop 1, L4 helix, and α4, as shown in Figure 7B. It is located at the connecting point between the $(\beta/\alpha)_8$ core and L4 hook-like structure of the second maltose-binding site (Figure 1). O-1 and O-2 of the acetate ion form hydrogen bonds with Asn 131 N-δ2 and O-δ1, respectively. O-1 of acetate forms additional hydrogen bonds with Gln 193 O and with water 623 which hydrogen bonds to O-γ1 of Thr 196. The side of the methyl group of the acetate is surrounded by hydrophobic residues, and it makes van der Waals contacts with the side chains of Tyr 175, Tyr 257, and Ile 260. Though the backbone structure of this acetate-binding site is conserved in both BCB and SBA, the side chain of Leu 213 in SBA, which correspond to Ala 199 in BCB, occupies the acetate-binding site. In addition, the

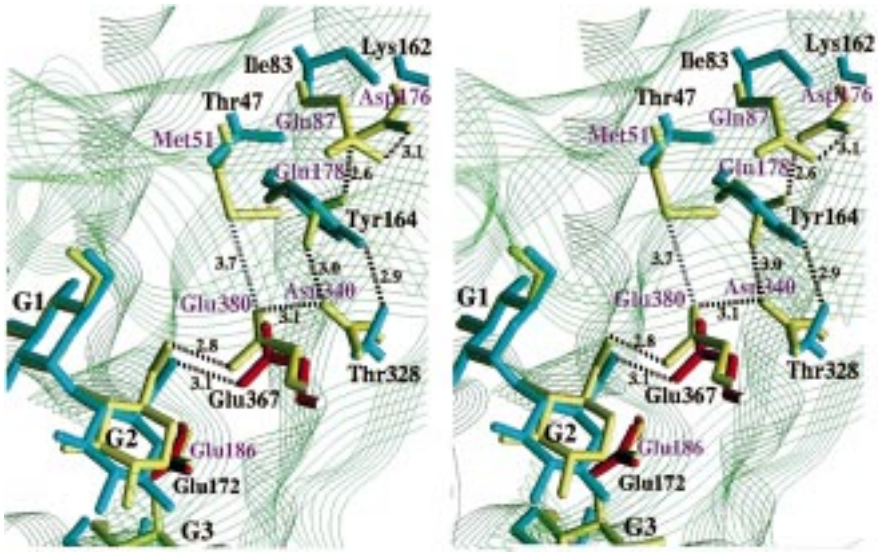

FIGURE 8: Stereodiagrams of the substituted residues on the Glu 367 side superimposed onto the SBA structure. The backbone structures of BCB are represented as a ribbon. The structures of BCB and SBA are represented as cyan and yellow lines, respectively. Two catalytic residues of BCB, Glu 172 and Glu 367, are red. G1, G2, and G3 denote the binding glucose residues. The hydrogen bonds are shown by broken lines.

substituted side chain of Asn 131−Thr 136 in SBA also seems to inhibit the binding of acetate to SBA (Figure 7B). The role of the bound acetate thus seems to stabilize the connecting region.

One sulfate exists at the beginning of α8 on the interface connecting a symmetry molecule (Figure 1). Its oxygen atom (O-1) hydrogen bonds to Asn 405 N and N-δ2, and also Lys 427 N-ζ of symmetry molecule 5. Since no direct hydrogen bonds between the symmetry molecules were observed except for Thr 26 O-γ1···C-terminal O of symmetry molecule 5 and no crystal appeared without sulfate, this sulfate seems to stabilize the crystal packing.

DISCUSSION

Positions of Maltose Molecules in the Active Site. In BCB−maltose complex, the positions of maltose molecules in the active site are slightly different from those reported for the SBA−maltose complex except for Glc 1 (Figure 4A). The positions of C-1 and O-5 of Glc 2 in the BCB−maltose complex are shifted toward the side chain of Glu 172 by 0.7 Å from the corresponding positions reported for the SBA−maltose complex (*17*). The distances between O-ε1 of Glu 367 and O-1 of Glc 2 and between O-ε1 of Glu 380 and O-5 of Glc 2 in the BCB−maltose complex are 4.8 and 3.8 Å, respectively. Consequently, there are no hydrogen bonds which correspond to those between O-ε1 of Glu 380 and O-5 of Glc 2 and between O-ε1 of Glu 380 and O-1 of Glc 2 found in the SBA−maltose complex (*17*). Instead of the direct hydrogen bonds found in the SBA−maltose complex, one water-mediated hydrogen bond was observed between O-ε1 of Glu 367 and O-1 of Glc 2 [Glc 2 O-1···Wat 679···Glu 367 O-ε1 (2.9 and 2.7 Å)]. The positions of Glc 3 and Glc 4 are also shifted toward the side chain of Tyr 186 by about 1 Å so that the distance between C-1 of Glc 2 and C-4 of Glc 3 becomes 0.64 Å longer than the corresponding distance found in the SBA−maltose complex (*17*). In the SBA−maltose complex, some occupancy of Glc 2 by a molecule of α-maltose was observed, suggesting the formation of maltotetraose (*17*). No density, however, was observed between Glc 2 and Glc 3 in the case of the BCB−maltose complex. These differences between the BCB−maltose and SBA−maltose complexes may be ascribed to the different protonation states between Glu 367 in BCB and Glu 380 in SBA. BCB−maltose complex data were collected at pH 4.6, whereas the structure of the SBA−maltose complex was determined at pH 5.4 (*17*). As the pK_a of Glu 380 in SBA is estimated to be 3.5 (*17*) and that of Glu 367 in BCB can be estimated to be around 5.5 from the pH−activity profile (*7*), Glu 367 in BCB seems to be protonated but Glu 380 in SBA is completely deprotonated. Thus, the glucose residue at subsite 2 in the BCB−maltose complex described here suggests the inactive form of which O-1 cannot interact directly with O-ε1 of Glu 367.

Different pH Optima between BCB and SBA. BCB has properties different from those of SBA in terms of optimum pH and specific activity, though they have a similar catalytic core domain. BCB has an optimum pH at around 7.0 in contrast to 5.4 in the case of SBA (*7*). The 1.5 pH unit shift in the optimum pH suggests a change in the pK_a values of the two catalytic residues, Glu 172 and Glu 367. As shown in Figure 4A, Glu 172 is located deep in the active site near the scissile glycosidic bond. On the other hand, Glu 367 is located on the side of the solvent, and near the OH-1 of the β-anomer glucose residue at subsite 2. These two Glu side chains act as an acid and base pair in the catalytic process as described for Glu 186 and Glu 380 of SBA (*16*). The residues around Glu 172 are well-conserved in β-amylase, except for Ala 289 in BCB which is substituted with Ser 297 in SBA. The side chain of Ala 289 makes van der Waals contact with O-ε2 of Glu 172 [Ala 289 C-β···Glu 172 O-ε2 (3.8 Å)]. In contrast, there are three substituted residues that exist around Glu 367 (Figure 8). These are Thr 47 (Met 51 in SBA), Tyr 164 (Glu 178), and Thr 328 (Asn 340). The side chain of Asn 340 in SBA forms a hydrogen bond with Glu 380 [Asn 340 N-δ2···Glu 380 O-ε2 (3.1 Å)], and the side chain of Met 51 on SBA exists near Glu 380 within a possible hydrogen bond [Met 51 S-δ1···Glu 380 O-ε2 (3.7 Å)]. In SBA, Glu 178 does not directly interact with Glu

380 [Glu 178 O-ϵ1···Glu 380 O-ϵ2 (4.9 Å)], but it forms a hydrogen bond with Asn 340 [Glu 178 O-ϵ1···Asn 340 O-δ1 (3.0 Å)], which in turn forms a hydrogen bond with O-ϵ2 of Glu 380 [Asn 340 O-δ1···Glu 380 O-ϵ2 (3.1 Å)]. Glu 178 in SBA also makes a hydrogen bond with Asp 176 [Glu 178 O-ϵ2···Asp 176 O-δ1 (2.6 Å)] which in turn forms a hydrogen bond with Gln 87 [Asp 176 O-δ1···Gln 87 O-ϵ1 (3.1 Å)]. This hydrogen bond network, including Glu 380, Met 51, Asn 340, Glu 178, Asp 176, and Gln 87, is not present in the BCB structure, suggesting that Glu 380 in SBA has a lower pK_a than Glu 367 in BCB by stabilizing the negatively charged form of Glu 380. The substitution of Ala 289 in BCB with Ser 297 in SBA also acts to increase the pK_a of Glu 178 by increasing the local dielectric constant.

On the Glu 367 side, the Thr-Tyr-Thr-Lys-Ile and Met-Glu-Asn-Asp-Glu pentads are conserved in the bacterial and plant type β-amylases, respectively, except for Ile in the bacterial enzyme (*16*). On the Glu 172 side, Ala 289 is partially conserved in some bacterial enzyme, though others have Ser at the corresponding residue (*16*). In the mutation study of barley β-amylase, the mutation of Ser 295 which correspond to Ala 289 in BCB to Ala increased the thermostability of the enzyme but seems to have little effect on the pH profile (*33*). Ser 295 in barley β-amylase is also responsible for the tight binding of Glc to subsite 3 (*34*). Thus, the side chains of Thr 47, Tyr 164, Thr 328, Lys 162, and Ile 83 are possible candidates for mutations that could control the optimum pH of BCB.

Strategy of Raw Starch Digestion by Bacterial β-Amylase. A comparison of the structures of BCB and SBA clearly demonstrated that BCB has an extra two maltose-binding sites which give the enzymes the ability to absorb and digest raw starch granules. These maltose-binding sites are located on the same side of the substrate-binding site about 32−37 Å from the catalytic site and about 58 Å from each other (Figure 1). One maltose-binding site is in the core L4 region which forms a hook-like structure. The other is in the C-terminal starch-binding domain and shares the same starch-binding site as that found in CGTase (*9*) and glucoamylase (*11*). In the starch-binding domains of CGTase and glucoamylase, two sugar-binding sites have been identified. The vacant second binding site in the BCB C-terminal domain suggests a reduced binding affinity due to substituted amino acids between 460 and 465. This C-terminal raw starch-binding domain also exists in some α-amylases, including maltotetraose-producing α-amylase (*5*, *8*). The Greek key structure of domain C in pancreatic and bacterial α-amylase also seems to play a role in raw starch binding. In contrast to the C-terminal raw starch-binding domain, the second maltose-binding site of BCB does not have any similarity to the sugar-binding site described for other amylases. This binding site is conserved only in bacterial β-amylase (*5*). The region of insertion and deletion around residues 211−242 in BCB suggests that plant β-amylase may have lost the structure during evolution.

To compare the topology of the starch-binding sites relative to the active site with that found in other amylases, the $(\beta/\alpha)_8$-barrel of BCB was superimposed onto those of other amylases exhibiting raw starch digestion. The superposition of the $(\beta/\alpha)_8$-barrel between BCB and CGTase shows an rms distance of 1.65 Å for 131 common C-α atoms within 2.5 Å. In this superposition, the second maltose-binding site and the binding site on the C-terminal domain in BCB are about 14 and 12 Å from the second binding site of CGTase domain E and the maltose-binding site of domain D (*9*), respectively. In addition, the C-terminal starch-binding domain of BCB corresponds to domain C of pancreatic α-amylase. It is noted that the same topology of starch-binding sites exists for both BCB and CGTase, though the domain structures of their starch-binding sites are completely different. This may suggest the importance of topology of the starch-binding site relative to the topology of the active site for efficient digestion of the raw starch granules.

ACKNOWLEDGMENT

Computation time was provided by the Supercomputer Laboratory, Institute for Chemical Research, Kyoto University.

REFERENCES

1. Thoma, J. A., Spradlin, E., and Dygert, S. (1971) *Enzymes (3rd Ed.) 5*, 115−189.
2. Kawazu, T., Nakanishi, Y., Uozuni, N., Sasaki, T., Yamagata, H., Tsukagoshi, N., and Udaka, S. (1988) *J. Bacteriol. 169*, 1564−1570.
3. Siggens, K. (1987) *Mol. Microbiol. 1*, 86−91.
4. Kitamoto, N., Yamagata, H., Kato, T., Tsukagoshi, N., and Udaka, S. (1988) *J. Bacteriol. 170*, 5848−5854.
5. Nanmori, T., Nagai, M., Shimizu, Y., Shinke, R., and Mikami, B. (1993) *Appl. Environ. Microbiol. 59*, 623−627.
6. Yamaguchi, T., Matsumoto, M., Shirakawa, M., Kibe, M., Hibino, T., Kozaki, S., Takasaki, Y., and Nitta, Y. (1996) *Biosci., Biotechnol., Biochem. 60*, 1225−1259.
7. Nanmori, T. (1988) in *Handbook of Amylases and Related Enzymes*, pp 94−99, Pergamon Press, Oxford, U.K.
8. Svensson, B., Jespersen, H. M., Sierks, M. R., and MacGregor, E. A. (1989) *Biochem. J. 264*, 309−311.
9. Lawson, C. L., Montfort, R., Strokopytov, B., Rozeboom, H. J., Kalk, K. H., de Vries, G. E., Penninga, D., Dijkhuizen, L., and Dijkstra, B. W. (1994) *J. Mol. Biol. 236*, 590−600.
10. Knegtel, R. M. A., Strokopytov, B., Penninga, D., Faber, O. G., Rozeboom, H. J., Halk, K. H., Dijkhuizen, L., and Dijkstra, B. W. (1995) *J. Biol. Chem. 270*, 29256−29264.
11. Sorimachi, K., Le Gal-Coeffet, M.-F., Williamson, G., Archer, D. B., and Williamson, M. P. (1997) *Structure 15*, 647−661.
12. Quian, M., Haser, R., and Payan, F. (1995) *Protein Sci. 4*, 747−755.
13. Quian, M., Spinelli, S., Driguez, H., and Payan, F. (1997) *Protein Sci. 6*, 2285−2296.
14. Larson, S. B., Greenwood, A., Cascio, D., Day, J., and McPherson, A. (1994) *J. Mol. Biol. 235*, 1560−1584.
15. Kadziola, A., Sogaard, M., Svensson, B., and Haser, R. (1998) *J. Mol. Biol. 278*, 205−217.
16. Mikami, B., Hehre, J. A., Sato, M., Katsube, Y., Hirose, M., Morita, Y., and Sacchattini, J. S. (1993) *Biochemistry 32*, 6836−6845.
17. Mikami, B., Degano, M., Hehre, E. J., and Sacchettini, J. S. (1994) *Biochemistry 33*, 7779−7787.
18. Nomura, K., Yoneda, I., Nanmori, T., Shinke, R., Morita, Y., and Mikami, B. (1995) *J. Biochem. 118*, 1124−1130.
19. Uozumi, N., Matsuda, T., Tsukagoshi, N., and Udaka, S. (1991) *Biochemistry 30*, 4594−4599.
20. Bernfeld, P. (1955) *Methods Enzymol. 1*, 149−158.
21. Mikami, B., Aibara, S., and Morita, Y. (1982) *Agric. Biol. Chem. 46*, 943−953.
22. Furey, W., and Swaminathan, S. (1997) *Methods Enzymol. 277*, 590−620.
23. Wang, B. C. (1985) *Methods Enzymol. 115*, 90−112.
24. Brünger, A. T. (1992) *A System for Crystallography and NMR*, *Yale* University Press, New Haven, CT.

25. Luzzati, V. (1952) *Acta Crystallogr. 5*, 802−810.
26. Ramakrishnan, C., and Ramachandran, G. N. (1965) *Biophys. J. 5*, 909−993.
27. Laskowski, R. A., MacArthur, M. W., Moss, D. S., and Thornton, J. M. (1993) *J. Appl. Crystallogr. 26*, 283−291.
28. Boel, E., Hjort, I., Svensson, B., Norris, F., Norris, K. E., and Fill, N. P. (1991) *EMBO J. 3*, 1097−1102.
29. Klein, C., and Schulz, G. E. (1991) *J. Mol. Biol. 217*, 737−750.
30. Sorimachi, K., Jacks, A. J., Le Gal-Coeffet, M.-F., Williamson, G., Archer, D. B., and Williamson, M. P. (1996) *J. Mol. Biol. 259*, 970−987.
31. Imberty, A., Chanzy, H., Pérez, S., Buléon, A., and Tran, V. (1988) *J. Mol. Biol. 201*, 365−378.
32. Machius, M., Wiegand, G., and Huber, R. (1995) *J. Mol. Biol. 246*, 545−559.
33. Yoshigi, N., Okada, Y., Sahara, H., and Koshino, S. (1995) *J. Biochem. 117*, 63−67.
34. Mikami, B., Yoon, H.-J., and Yoshigi, N. (1998) *J. Mol. Biol. 285*, 1235−1243.
35. Mikami, B., Morita, Y., and Fukazawa, C. (1988) *Seikagaku 60*, 211−216.
36. Adachi, M., Mikami, B., Katsube, T., and Utsumi, S. (1998) *J. Biol. Chem. 273*, 19859−19865.
37. Nicholls, A., Sharp, K. A., and Honig, B. (1991) *Proteins 11*, 281−296.

BI9829377